Journal of Materials Chemistry A

Accepted Manuscript

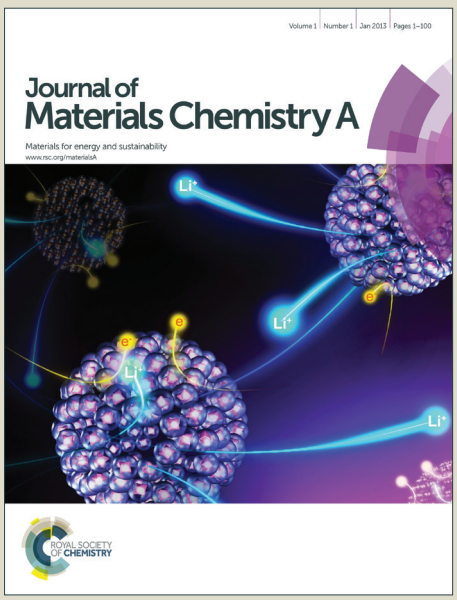

ROYAL SOCIETY OF CHEMISTRY

www.rsc.org/materialsA

Journal Name

RSCPublishing

ARTICLE

A Carbon Modified $NaTaO_3$ Mesocrystal Nanoparticle with Excellent Efficiency of Visible Light Induced Photocatalysis

Cite this: DOI: 10.1039/xoxxoooooox

Received ooth January 2012,
Accepted ooth January 2012

DOI: 10.1039/xoxxoooooox

www.rsc.org/

Xiaoyong Wu, Shu Yin*, Bin Liu, Makoto Kobayashi, Masato Kakihana, Tsugio Sato

A carbon modified $NaTaO_3$ mesocrystal nanoparticle (ca. 20 nm) was successfully synthesized by a one-pot solvothermal method, employing $TaCl_5$ and NaOH as the starting materials and distilled water/EG mixed solution as a reaction solvent in the presence of appropriate amounts of glucose. The mesocrystal sample presented such high specific surface area as 90.8 m^2g^{-1} with large amounts of well-dispersed mesopores in the particle, owing to the co-effect of EG and glucose during the reaction process. A non-classic formation mechanism was proposed for the growth of $NaTaO_3$ mesocrystal. Furthermore, the $NaTaO_3$ mesocrystal exhibited much improved visible light absorption in addition to the intrinsic UV light absorption as a result of carbon modification originated from glucose. Based on the large specific surface area, high crystallinity and optical property, the carbon modified $NaTaO_3$ mesocrystal demonstrated excellent efficiency for the continuous NO gas destruction under the irradiation of UV, short wavelength visible lights (>400 m) and even long wavelength visible light (>510 nm), much superior to those of unmodified $NaTaO_3$ specimen and commercial titania, P25. The carbon modified $NaTaO_3$ mesocrystal nanoparticles prepared in this work would probably have a potential utilization in the environmental purification and energy conversion.

Introduction

Mesocrystal, that is defined as a colloidal crystal in which all elemental units grow oriented in the same crystallographic direction to form an ordered superstructure, has drawn increasing attention from researchers and is warmly expected to be used as catalysts, electrodes, optoelectronics, sensors, biomedical materials, lightweight structural materials, etc. due to its unique properties with nanoparticulate, mesoporous and single crystal-like structure.[1-6] In recent years, many methods have been developed to synthesize fascinating mesocrystals, which can be mainly divided into three types. The one is to use a template to produce mesoporous in the target crystal. [7, 8] For instance, Kohiku et al. fabricated the $BaTiO_3$ and $SrBi_2Ta_2O_9$ mesocrystals by utilizing the MCM-41 molecular sieve as a mesoporous template.[7] However, due to the utilization of template in the synthesis process, a high temperature calcination or other special process is generally required to remove the template from the final mesocrystal. The second category of the preparation way for mesocrystals is topotactic transformation, where the special precursors or intermediates are thermally transferred to expected mesocrystal oxides. [9, 10] Zhou et al. successfully synthesized mesocrystal TiO_2 through topotactically transformed NH_4TiOF_3 crystals.[9] Nevertheless, this process usually demands special precursors and high temperature calcination. In addition, its products are limited in the binary metal oxides and hard for ternary metal oxides. The third and most commonly used one is oriented aggregation via self-assembling.[11, 12] Because the mesocrystals prepared by this process dominantly presents uniform size, larger specific surface area and well dispersed mesopores, which are of great importance for many applications. Zhang et al. reported the preparation of a uniform CuO nanoparticle with perfectly dispersed mesopore in the crystal by a typical oriented-aggregation process, which was needed to firstly prepare Cu related complex via a complex way. [11] Despite many virtues of this process, special conditions, precursors or complex procedure is extensively existed in the preparation routine.[3, 13] Therefore, much more progress is still needed to synthesize the mesocrystal with high efficiency.

Perovskite structured $NaTaO_3$ has become one of the most promising photocatalysts due to its peculiar electronic structure in the application of water splitting and toxic pollutant

decomposition. [14-16] However, there are two main factors limited the high efficiency of $NaTaO_3$ in photocatalysis. On one hand, the wide intrinsic band gap of $NaTaO_3$ (ca. 3.8 eV) restricts the widespread utilization in the visible light induced photocatalytic performance.[17-19] On the other hand, the particle size of $NaTaO_3$ prepared by many reported works are still large, indicating relatively small specific surface area and subsequent confined photocatalytic activity.[15, 19, 20] In order to increase the specific surface area of the samples, the mesoporous structure should be a candidate strategy. However, the research about the preparation of mesoporous $NaTaO_3$ is very few. Cui et al. prepared the $NaTaO_3$ porous polycrystal microspheres with the large specific surface area of 57.8 m^2g^{-1},[21] which is much larger than the common one about 10 m^2g^{-1}.[14, 19] But two complex steps and special device are needed for the preparation of mesoporous $NaTaO_3$ in the related study. Meanwhile, the prepared $NaTaO_3$ presented polycrystal instead of mesocrystal, and only exhibited UV light induced photocatalytic property. In addition, Sun et al. reported a simple approach to prepare strontium sodium tantalite mesocrystals with the specific surface area of ca. 40 m^2g^{-1}.[22] Nevertheless, the high calcination temperature is indispensable. In addition, the prepared mesocrystals still showed the relatively larger particles about several hundreds of nanometers with serious agglomeration, and the mosopore was not well dispersed. Moreover, the photocatalytic activity was also limited in the UV light range. Therefore, a more facile and efficiency approach to synthesize small particle size of $NaTaO_3$ mesocrystal with superior visible light responsive photocatalytic performance was still strongly required.

Herein, a carbon modified $NaTaO_3$ mesocrystal nanoparticle with high efficiency of visible light driven NO gas destruction activity ($deNO_x$) was prepared by a facile one-pot solvothermal method using $TaCl_5$ and NaOH as starting materials, ethylene glycol (EG) and distilled water mixed solution as a solvent in the presence of glucose. The glucose was not only employed as the carbon-related matertials resource, but also plays an essential role in the formation and dispersion of uniform sample particles and mesopores in the monocrystal. The non-classic oriented aggregation mechanism via a self-assembly was proposed for the formation of mesocrystal in this work.

Experimental

Sample preparation

A series of carbon modified $NaTaO_3$ mesocrystals were prepared by a simple solvothermal method. In a typical procedure, 2 g glucose were ultrasonically dispersed in 60 mL distilled water/EG (30:30) mixed solution for 15 min. After that, 0.1 g $TaCl_5$ was added into the mixed solution with magnetic stirring for 30 min, following by the addition of 2.4 g NaOH. After another 60 min magnetic stirring, the mixed solution was transferred into a 100 mL Teflon-lined stainless steel autoclave and heat-treated at 180 ^oC for 20 h. Eventually, the powders were centrifuged, washed and dried in a vacuum at 60 ^oC overnight. The samples prepared by using different amounts of glucose (0, 1, 2 and 2.5 g) were denoted as $NaTaO_3$-E-G0, $NaTaO_3$-E-G1, $NaTaO_3$-E-G2 and $NaTaO_3$-E-G2.5, respectively.

For comparison, the sample $NaTaO_3$-W-G2 was synthesized by using 60 mL pure distilled water as a reaction solvent instead of distilled water/EG mixed solution, while other conditions were the same as $NaTaO_3$-E-G2. The sample $NaTaO_3$-W-G0 was prepared by the same procedure as $NaTaO_3$-W-G2 solely without the addition of glucose. The sample $NaTaO_3$-E-G2-500 was also synthesized by calcining sample $NaTaO_3$-E-G2 at 500 ^oC for 2 h. In addition, a controllable sample $NaTaO_3$-PE-G0 was also fabricated by the same solvothermal method using pure 60 mL EG as reaction solvent without the addition of glucose.

Characterization

The crystalline phases of the samples were determined by X-ray diffraction analysis (XRD, Bruker AXS D2 Phaser) with graphite-monochromized CuKα radiation. The UV–vis diffuse reflectance spectra (DRS) of products were checked by a UV–vis spectrophotometer (Shimadazu, UV-2450). The specific surface areas and pore distribution of powders were evaluated via the BET method (Quantachrome Instruments, NOVA4200e). The size and morphology of the specimens were examined by transmission electron microscopy (TEM, JEOLJEM-2010). In addition, the porous structure and selected area electron diffraction (SEAD) pattern of the mesocrystals were observed by high resolution transmission electron microscopy (HRTEM, FE-TEM, JEM-2100F). FT-IR measurements were conducted to check the surface status of samples by using the FTS7000 series (DIGILIB). The surface composition and binding energy of the samples were investigated by X-ray photoelectron spectroscopy (XPS, Perkin Elmer PHI 5600). The shift of the binding energy owing to relative surface charging was calibrated by the C 1s level at 284.6 eV and Ar^+ sputtering was also utilized to clean the surface of samples. The Raman spectra of samples were carried out on a NRS-3300FL series Raman spectrometers equipped with visible (532 nm) laser excitation. Organic elementary analysis was used to determine the amount of carbon in the samples by a Micro Cordor JM10 device. The TG-DTA (Rigaku, TG8101D) was performed on the samples with a heating rate of 10 ^oC/min in air. The photoluminescence spectra of samples were tested by a spectrofluorometer (Shimadzu RF-5300P).

Photocatalytic activity tests

The photocatalytic performance of the $NaTaO_3$ based samples was evaluated by investigating the destruction of continuous NO_x gas ($DeNO_x$) in a flow type reactor with the irradiation of a 300 W simulated solar light (ASAHI SPECTRA HAL-302) at room temperature. The sample powder was spread in a hollow (20 mm*16 mm*0.5 mm) of glass plate and then fixed at the bottom center of the reactor (373 cm^3 of internal volume), in which a 1:1 mixed gas of air and nitrogen based 1 ppm of NO

was continuously flowed with the rate of 200 cm3 min-1. Before measurement, the sample was kept in the dark for 30 min to reach an adsorption and desorption equilibrium of NO gas. Subsequently, the sample was irradiated by the simulated solar light, where the light wavelengths of irradiation were tuned by different filters: Pyrex glass for > 290 nm, Kenko L41 Super Pro (W) filter > 400 nm and Fuji triacetyl cellulose filter >510 nm. The measuring time for each sample under each wavelength was 10 min. [23] Finally, the concentration of NO gas at the outlet of reactor was checked by a NOx analyzer (Yanaco, ECL-88A).

Results and discussion

Figure 1 shows the XRD patterns of the carbon modified $NaTaO_3$ specimens prepared under different conditions. It is clear that the sample $NaTaO_3$-E-G0 (Fig.1 (a)) synthesized by distilled water/EG mixed solution in the absence of glucose could be indexed well to the orthorhombic phase of $NaTaO_3$ (JCPDS file No. 25-0863) with high crystallinity. After the addition of glucose, the sample $NaTaO_3$-E-G2 (Fig.1 (b)) also presented the pure $NaTaO_3$ phase but with decreased intensity of diffraction peaks, suggesting the formation of smaller particle size of products in the presence of glucose. In addition, as the glucose was still employed but the mixed solution was replaced by pure distilled water, some impurity peaks belonged to $Na_2Ta_2O_6$, which is an intermediate phase in the formation of $NaTaO_3$ phase, were appeared in the sample $NaTaO_3$-W-G2 (Fig.1 (c)), indicating the existence of EG in the reaction solution was favourable for the production of $NaTaO_3$ phase with relatively small particle size. Additionally, the amplified XRD patterns of these three samples in the range of 20-35° were also illustrated in Fig. S1. It is apparent that in addition to the difference between the relative intensity of peaks, there was no obvious peak shift observed for these three samples, indicating that the carbon was probably not doped into the $NaTaO_3$ crystal lattice. On the other hand, the effect of glucose content on the crystallinity of $NaTaO_3$ was also investigated in the Fig. S2. With the increase of glucose addition up to 1 and 2 g, the samples $NaTaO_3$-E-G1 and $NaTaO_3$-E-G2 still presented the pure $NaTaO_3$ phase but the peak intensity was decreased, while as the glucose content was enhanced up to 2.5 g, the intermediate phase, $Na_2Ta_2O_6$ was induced, meaning that the addition of glucose in the reaction solution was only in favor of producing small size powder but detrimental for the formation of $NaTaO_3$ phase. Therefore, it can be deduced from the above XRD results that the coexistence of EG and glucose in the reaction solution was strongly desirable for the formation of pure $NaTaO_3$ phase with small particle size.

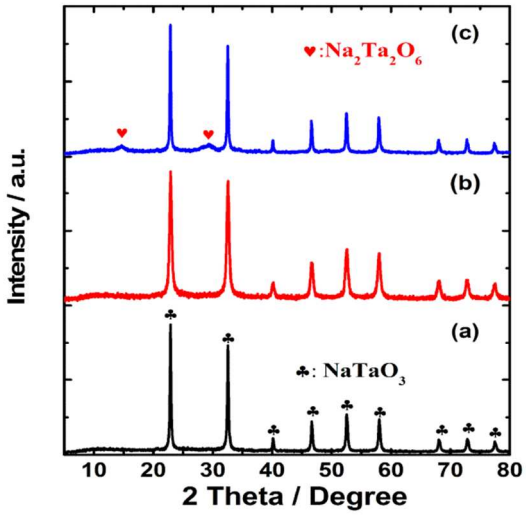

Fig. 1 XRD patterns of samples $NaTaO_3$-E-G0 (a), $NaTaO_3$-E-G2 (b) and $NaTaO_3$-W-G2 (c) prepared under various reaction conditions.

The corresponding TEM images of the carbon modified $NaTaO_3$ samples fabricated under various conditions are exhibited in Fig. 2, and the corresponding reaction conditions, surface areas, pore sizes and volumes of samples were listed in Table 1. In Fig. 2 (a), the $NaTaO_3$-E-G0 particles synthesized by mixed solution in the absence of glucose presented agglomeration, to some extent, with non-uniform sizes. Meanwhile, some mesopores were also existed in the part of particles with the pore size of 4.0 nm as well as pore volume of 0.180 $cc \cdot g^{-1}$ as shown in Table 1. When the glucose was employed, it is apparent that the particles of sample $NaTaO_3$-E-G2 were well dispersed with relatively uniform size about 20 nm as shown in Fig. 2 (b). Moreover, the specific surface area of the sample $NaTaO_3$-E-G2 was significantly increased to 90.8 m^2g^{-1}, which is about four times higher than that of sample $NaTaO_3$-E-G0, and also much larger than the reported values for most of $NaTaO_3$ particles.[15-22] This might be owing to the much decreased particle size with well distribution, resulting to homogeneous pore structure with pore size of 7.8 nm and much improved pore volumes (0.362 $cc \cdot g^{-1}$). However, when the EG was removed from the reaction solution for the sample $NaTaO_3$-W-G2 in Fig. 2 (c), the particle size greatly increased to about 100 nm together with the decrement of surface area (50.2 m^2g^{-1}), while some smaller pores (3.6 nm) were still remained in the inner of particles.

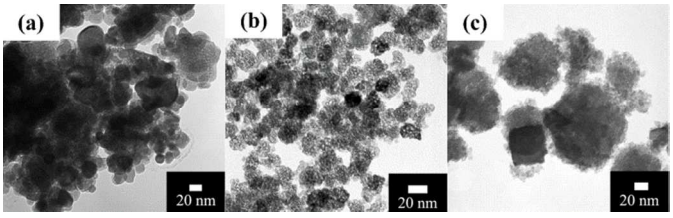

Fig. 2 TEM images of $NaTaO_3$-E-G0 (a), $NaTaO_3$-E-G2 (b) and $NaTaO_3$-W-G2 (c).

Table 1. The reaction conditions and physical properties of $NaTaO_3$-E-G0, $NaTaO_3$-E-G2, $NaTaO_3$-W-G2.

Samples	Reaction solution	Glucose (g)	Surface area (m^2g^{-1})	Pore size (nm)	Pore volume ($cc \cdot g^{-1}$)
$NaTaO_3$-E-G0	Water/EG	0	22.7	4.0	0.180
$NaTaO_3$-E-G2	Water/EG	2	90.8	7.8	0.362
$NaTaO_3$-W-G2	Water	2	50.2	3.6	0.152

In order to investigate the effect of glucose and EG on the formation of small particle size and mesoporous structure of the samples, some TEM images of the carbon modified $NaTaO_3$ with respect to different amounts of glucose and the sample $NaTaO_3$-W-G0 prepared by pure distilled water without the addition of glucose are also shown in the Fig. S3 and Fig. S4, respectively. As shown in Fig. S3, with the increase of glucose content in the reaction solution, the particle became smaller and more uniform with large amounts of mesopores. Nevertheless, as the glucose content was increased to 2.5 g, the morphology of particle was broken and become more irregular. As for sample $NaTaO_3$-W-G0, it presented relatively serious agglomeration with the particle size of ca. 75 nm and no obvious mesopores were observed in the particles. Moreover, the XRD pattern and TEM image of the control sample $NaTaO_3$-PE-G0 prepared by pure EG solution in the absence of glucose were complemented in Fig. S5. $NaTaO_3$-PE-G0 still presented pure orthorhombic $NaTaO_3$ phase but with very poor crystallinity and irregular, agglomerated particles. Meanwhile, the product yield of $NaTaO_3$-PE-G0 powders was such low that it cannot make other characterizations. All of these should be owing to the low solubility of NaOH and poor reaction rate between NaOH and $TaCl_5$ in the pure EG solution. Based on above description, it could be learned that the coexistence of glucose and EG in the reaction solution were greatly favourable for the formation of small size of particles decorated with large amounts of mesopores.

Figure 3 shows the particle size and morphology of the sample $NaTaO_3$-E-G2 with different magnifications. It is explicit that the $NaTaO_3$-E-G2 particles displayed uniform distribution with soft agglomeration. More importantly, the mesopores could be clearly confirmed in all of well-dispersed particles, indicating the existence of perfect mesoporous nanostructure. Figure 4 shows corresponding nitrogen adsorption-desorption isotherms and pore size distribution plots of the sample $NaTaO_3$-E-G2. The isotherm of the sample was a typical IV type with H3 hysteresis loops, implying the mesoporous structure.[24]

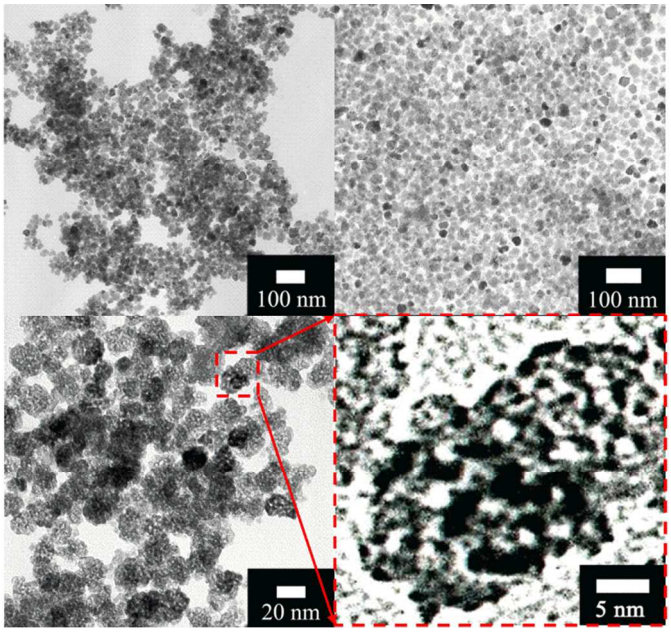

Fig. 3 TEM images of sample $NaTaO_3$-E-G2 with different magnifications.

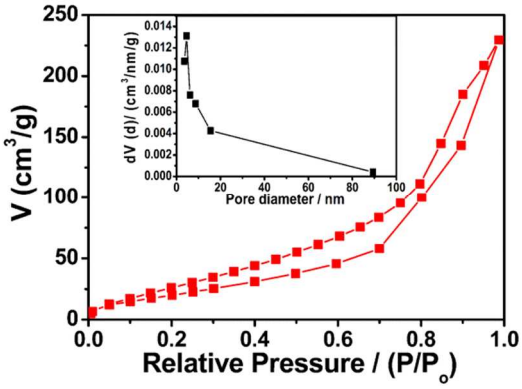

Fig. 4 Nitrogen adsorption-desorption isotherms and the corresponding pore size distribution plots (inset) of $NaTaO_3$-E-G2.

Additionally, a focus technique in TEM measurement was employed to further investigate the mesoporous structure in the inner of sample particles. Figure 5 (a), (b) and (c) show the TEM images of $NaTaO_3$-E-G2 examined under various focus circumstances. It is well acknowledged that under the overfocus status, the black area in the inner of particles is attributed to the fringe of substance and space. While under the underfocus condition, it is contrary that the white area in the inner of particles is assigned to the fringe of substance and space, and the in-focus is the normal condition as we take a picture.[25] So it could be found that under overfocus and underfocus conditions, a lot of discrete black-and-white areas existed in the interior of the particles, respectively, confirming that huge number of continuous mesopores truly existed in the particles.

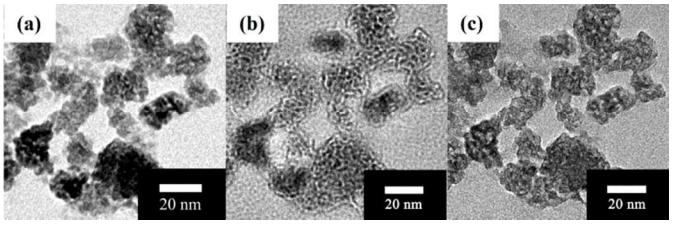

Fig. 5 TEM images of sample $NaTaO_3$-E-G2 evaluated by different focus conditions: in-focus (a), overfocus (b) and underfocus (c).

Figure 6 presents the HRTEM images and SAED pattern of sample $NaTaO_3$-E-G2 in different areas. It was clear that the single sample particle (ca.20 nm) exhibited well-defined crystallinity and regular lattice fringe with lattice spacing of 0.378 nm corresponded to (101) plane of orthorhombic phase $NaTaO_3$, indicating the small nanounits oriented growth along the same direction. Furthermore, the two red square areas, covering nearly a single particle, have been analysed by the SAED. The SAED results clearly confirmed that both of these two areas exhibited the single crystal-like patterns as shown in the yellow squares of Fig. 6. As we all known, mesocrystal should have two features including mesoporous structure and single crystal-like patterns. In this work, these two features have been nicely confirmed by Figs. 3, 4, 5 and 6. Therefore, it could be learned that a well-dispersed mesocrystal $NaTaO_3$ nanoparticle has been successfully prepared by the facile solvothermal method using distilled water/EG as the solvent in the presence of appropriate amounts of glucose.

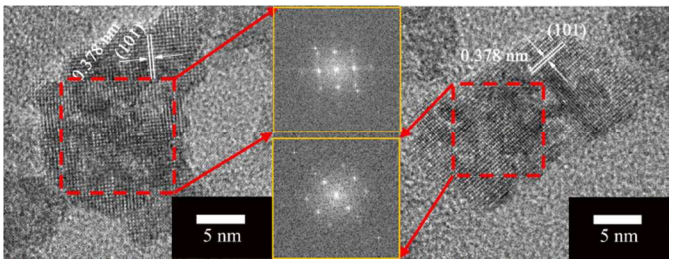

Fig. 6 HRTEM images and SAED patterns of sample $NaTaO_3$-E-G2.

Meanwhile, the corresponding possible formation mechanism of nanoscale mesocrystals for $NaTaO_3$-E-G2 was proposed as shown in Fig. 7. Firstly, the starting materials $TaCl_5$ and NaOH in distilled water/EG mixed solution started to form nucleation clusters with the increment of temperature, then gradually grew up until the critical size of crystal nucleus. In the next step, generally speaking, the further growth of primary particles is according to the role of large particles fused smaller particles by ion-by-ion attachment and unit cell replication, so called Ostwald ripening process driven by the surface energy reduction.[26, 27] While another non-classic oriented aggregation growth mechanism was also proposed by many researchers for the formation of mesocrystals in the presence of an organic stabilizer, where the larger particle is obtained by self-assembling or self-aggregating of the adjacent small nanparticles, which shared the same crystallographic orientation and were connected by organic additives or amorphous materials.[3, 13, 26, 27] The motivation for this oriented attachment process is induced by removing numerous high energy surfaces and finally leading to the total reduction in the surface free energy. In the oriented aggregation process, the rate of particle growth via self-assembly is much higher than that of the ion-by-ion attachment so that the self-assembly can be predominance in the further growth of nanoparticles.[26] In this work, the non-classic oriented aggregation process was employed. It is well known that the EG is commonly used as a stabilizer to synthesize some special shape of nanoparticles.[29] There are also a lot of hydroxyl radicals in the glucose, which should have the similar function as that of EG. Therefore, as the nucleation clusters grew to the critical size, the primary nanoparticles could be temporarily stabilized by the EG or glucose in the reaction solution simultaneously. Finally, the stabilized nanoparticles would be self-assembled by the surface organic additives to form a mesocrystal. The formation of well-dispersed mesocrystal with a large amount of mesopores should be the co-effect of the EG and appropriate glucose content. The glucose not only played the partial role of the stabilizer but also was of great importance for small particle size and well-dispersion of mesocrystals as shown in Fig. 2 and Fig. 3. It is accepted that the mesocrystal is a metastable phase, which can be further fused to form a single crystal along with the disappearance of mesoporous in the drive of thermal energy. So the sample $NaTaO_3$-E-G2-500 was also treated by annealing the mesocrystal $NaTaO_3$-E-G2 at 500 °C, and the corresponding TEM images was presented in Fig. S6. There was no apparent mesopores observed for $NaTaO_3$-E-G2-500 particles, further indirectly confirming the formation of mesocrystal for the sample $NaTaO_3$-E-G2.

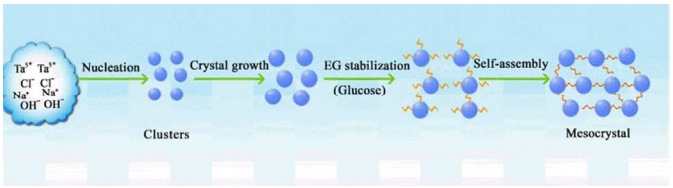

Fig. 7 Formation mechanism of carbon modified $NaTaO_3$ mesocrystal.

Figure 8 shows the DRS, FTIR spectra and XPS of the samples prepared under different conditions. It was found that the sample $NaTaO_3$-E-G0 exhibited mainly UV light absorption with a little bit visible light absorption induced by the modification of EG on the optical property of $NaTaO_3$,[14] while as the glucose was added for the synthesis of samples $NaTaO_3$-E-G2 and $NaTaO_3$-W-G2, the visible absorption capability was significantly improved (as shown in Figure 8 (a)), which might be due to the carbon modification of the $NaTaO_3$ surface. It could be confirmed from FTIR spectra in Figure 8 (b) that there were three new carbon-related peaks appeared on the surface of samples with the addition of glucose. The peak located at 1593 cm^{-1} was ascribed to the hydrogen-bonded carbonyl stretching.[30] The peak situated at 1357 cm^{-1} was assigned to the angular deformation of C-H,[31] while the peak formed at 1089 cm^{-1} was attributed to the C-C stretching of carbohydrates.[32] In

addition, the DRS and FTIR spectra of samples prepared by various glucose contents were also presented in Fig. S6-(a) and (b), respectively. With the increase of glucose concentration, the visible light absorption increased and the corresponding intensity of related peaks also enhanced, indicating the glucose was truly helpful for the enhancement of visible light absorption by changing the surface status. As shown in Fig. 8 (c), the XPS analysis revealed that both of samples $NaTaO_3$-E-G0 and $NaTaO_3$-E-G2 displayed three same peaks at 284.4, 285.8, 288.0 eV. The 284.4 eV peak was corresponded to the adventitious carbon, and the peak located at 288.0 eV was indicated to the C-O bond related species, which was probably induced by the modification of EG on the samples.[14, 33-35] While the peak lied at 285.8 eV was as a result of carbon-related materials, which presented the similar binding energy with that of carbon in the graphite intercalation compounds, [36, 37] and could also get from the atmosphere or the reaction circumstance. Meanwhile, it can be seen that the relative area of 285.8 eV peak in the sample $NaTaO_3$-E-G2 was much larger than that of sample $NaTaO_3$-E-G0, indicating that in addition to partially from the atmosphere, the carbon-related material was also originated from the addition of glucose or EG in the reaction solution. Furthermore, according to Qian Li et al.'s report,[38] the C 1s related peak shift should be observed to some extent when the C was doped into the sample lattice. However, in this work, there was no obvious C 1s peak shift observed for both samples and also no corresponding diffraction peak shift happened in the XRD pattern of samples as displayed in Fig. S1, indicating that the C probably covered on the surface of sample particles with the form of carbonaceous species instead of doping in the $NaTaO_3$ crystal lattice. In addition, the chemical bonding between Ta and C around 22.5eV could not be observed, also indicating carbon was not doped into the lattice of $NaTaO_3$.The XPS survey spectra of these two samples are also displayed in Fig. S7. The sample $NaTaO_3$-E-G2 also exhibited much higher C 1s peak intensity than that of sample $NaTaO_3$-E-G0, implying much more carbon-related substances existed in the sample $NaTaO_3$-E-G2. It is well known that the glucose is commonly used to prepare spherical carbon particles by the solvothermal or hydrothermal method. [39, 40] In our case, there was no obvious carbon formation after the solvothermal reaction with the addition of glucose. However, when the solution was heat-treated in the same condition without the addition of NaOH, a great deal of carbon was appeared in the final solution, indicating that the transformation from glucose to carbon could be significantly hindered in the basic circumstance, and the detailed reasons for this phenomenon is still unclear, which would be our next work. From this, it could be induced that a trace of carbonaceous species has been produced in the sample $NaTaO_3$-E-G2 with the presence of glucose, finally leading to the high visible light absorption activity of the sample. The TG and organic elementary analysis were conducted to check the content of C in the samples. Fig. 9 plots the TG curves of samples from the room temperature to 1000 °C. There were three steps of weight loss existed. The first weight loss from room temperature to ca. 250 °C was ascribed to the elimination of absorbed water. The second loss stage from 250 to 450 °C should be attributed to the decomposition of carbonaceous species on the surface of samples. For the sample $NaTaO_3$-E-G0, about 1.17% weight was lost, probably originating from the residue EG or similar organic materials on the surface of sample. Regarding sample $NaTaO_3$-E-G2 in the presence of glucose, appropriate 4.15% of sample was lost in this process. The corresponding carbonaceous species should be produced from EG and glucose

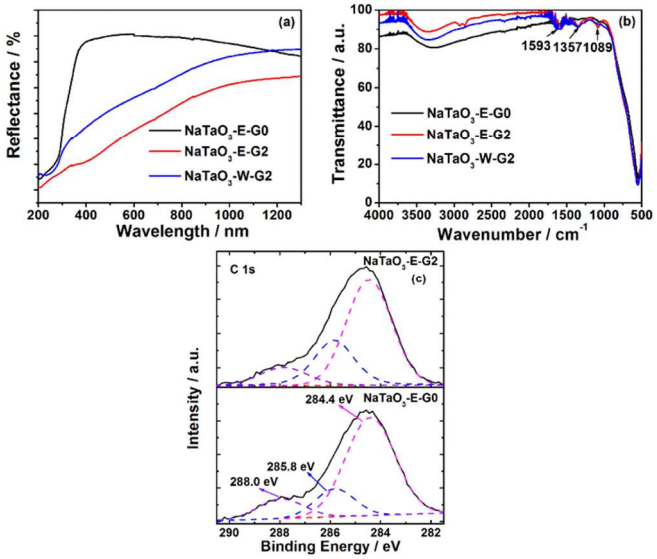

Fig. 8 DRS (a), FTIR spectra (b) of samples $NaTaO_3$-E-G0, $NaTaO_3$-E-G2 and $NaTaO_3$-W-G2 and XPS spectra of C 1s of samples $NaTaO_3$-E-G0, $NaTaO_3$-E-G2 (c).

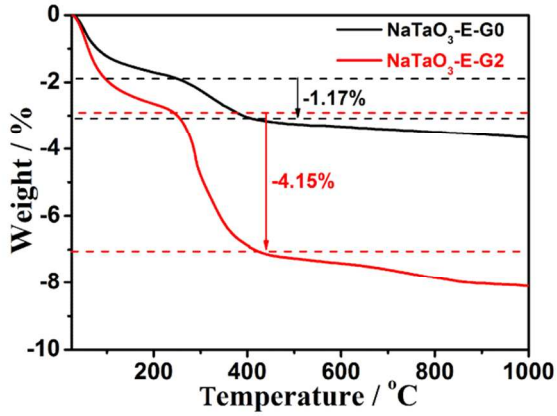

Fig. 9 TG profiles of samples $NaTaO_3$-E-G0 and $NaTaO_3$-E-G2.

in the reaction. However, according to the organic elementary analysis, only 0.52 and 2.15% of C were determined in the samples $NaTaO_3$-E-G0 and $NaTaO_3$-E-G2, respectively. These contents were much lower than the results from TG, indicating the C were existed as the carbon related compounds rather than C solely. These results can indirectly confirm that the carbon was not doped into the $NaTaO_3$ crystal lattice. The last stage from 450 to 1000 °C was probably assigned to the remove of

surface hydroxyl.[41] Besides, the Raman spectra of samples $NaTaO_3$-E-G0, $NaTaO_3$-E-G2, $NaTaO_3$-W-G2 and $NaTaO_3$-W-G0 were also added in Fig. S8. It was worth noting that this analysis was carried out after laser irradiation for long time to eliminate some of substance on the surface of samples. Because there was strong luminescence disturbance existed in the Raman spectra for samples $NaTaO_3$-E-G0, $NaTaO_3$-E-G2, $NaTaO_3$-W-G2 and no peaks were observed in the test range under the condition of investigation without laser irradiation. Even after the long irradiation, the peaks corresponding to $NaTaO_3$ powder were still weak. Moreover, the sample $NaTaO_3$-E-G2 presented the weakest peaks whereas the sample $NaTaO_3$-W-G0 exhibited the strongest peaks, which were nicely indexed to the relative C related contents in samples. So it can be deduced that the luminescence disturbance in the Raman analysis probably be owing to the existence of carbonaceous species on the surface of samples, further determining that the C was existed as a form of absorbed C related compound instead of dopant in the samples.

With the development of science and technology, the air pollution has become a serious problem. In order to deal with this issue especially for toxic NO_x gas, many techniques have been proposed such as selective catalytic reduction (SCR), filter, non-thermal plasma and photocatalysis, etc.. The SCR has an advantage of high efficiency for the destruction of NO_x gas over other methods. However, it usually needs relative high reaction temperature, extra ammonia as a reductant, and complex system. Filter is commonly utilized to physically deal with the particulate matter for the exhaust gas released from vehicle, which requires further technique to remove the absorbed contaminant. As for non-thermal plasma, it also presents high efficiency of $deNO_x$ ability. Nevertheless, it is generally not alone used and needs to combine with catalyst. Furthermore, it requires special high local electrical field and finally leads to fuel penalty for the vehicle. In addition, the above mentioned three strategies are commonly used in the vehicle with limited application space. However, the NO_x gas poison is dispersed in the whole air and a large-scale and low-cost technique is still strongly required. The photocatalysis as a green chemical method has been of great concern due to its high efficiency, low-cost, facile, environmental benign. It has been widely used in the wall of building, road, tunnel, etc..[42-44] In this work, the destruction of continuous NO_x gas was employed to investigate the photocatalytic activity of samples under the irradiation of various wavelengths of lights. Figure 10 (a) and (b) show the $deNO_x$ ability for the samples prepared under the different reaction conditions. The sample $NaTaO_3$-E-G0 presented the similar $deNO_x$ activity as commercial titania, P25 under the irradiation of simulated solar light with different filters. The visible light responsive activity of the sample $NaTaO_3$-E-G0 was induced by the EG modification, which has been systematically researched in our previous work.[14] As for the visible light driven photocatalytic

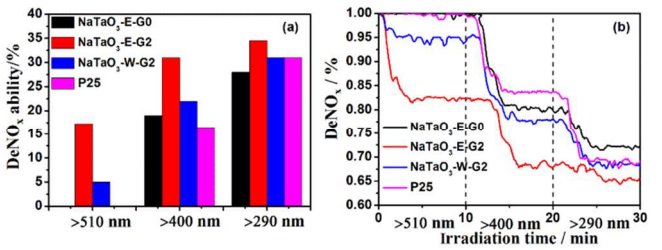

Fig. 10 $DeNO_x$ ability of $NaTaO_3$-E-G0, $NaTaO_3$-E-G2, $NaTaO_3$-W-G2 (a) and the time dependence of NO_x destruction activity of relevant samples (b) as well as those of P25 under the irradiation of different wavelengths of lights.

performance of P25, it should be owing to the impurity contaminations in the P25 powders.[33, 45] While as the glucose was introduced in the synthesis process of the sample $NaTaO_3$-E-G2, it revealed that not only nice UV and short wavelength visible lights (>400 nm) induced photo-activity but also the excellent $deNO_x$ efficiency under the irradiation of long wavelength visible light above 510 nm, i.e., about 17.0% NO destruction, which was much superior to sample $NaTaO_3$-E-G0 and P25. The high activity of this sample should be due to the outstanding visible light absorption as shown in Fig. 8 (a) and extremely high specific surface area as listed in the table 1. The sample $NaTaO_3$-W-G2 fabricated by the pure distilled water in the presence of glucose displayed higher performance than the sample $NaTaO_3$-E-G0 and P25, especially under the irradiation of visible light. However, it was much less effective in comparison with that of $NaTaO_3$-E-G2, mainly owing to the much decreased specific surface area of sample $NaTaO_3$-W-G2 (see Table 1). Additionally, the effect of glucose content on the photocatalytic property of carbon modified $NaTaO_3$ samples was also plotted in the Fig. S9, which well suggested the positive influence of glucose on the total photocatalytic performance of samples. It is well known that the high efficiency of photocatalysis is generally determined by light absorption capability, specific surface area and the separation ability of charge carriers. In this work, the sample $NaTaO_3$-E-G2 presented the highest $deNO_x$ ability over other samples. Compared with sample $NaTaO_3$-W-G2, sample $NaTaO_3$-E-G2 revealed the similar UV and visible light absorption ability but with much higher specific surface area as shown in Fig. 8 (a) and Table. 1. Meanwhile, the photoluminescence spectra of the samples were also represented in Fig. S10 to investigate the separation ability of charge carriers.[46,47] It can be learned that the sample $NaTaO_3$-E-G2 also exhibited similar separation ability with that of the sample $NaTaO_3$-W-G2, but much poorer than that of sample $NaTaO_3$-E-G0 which implied that the C modification was not made a positive effect on the separation ability of the samples. From above discussion, it might be concluded that the high specific surface area finally led to the outstanding $deNO_x$ ability of sample over the factors of light absorption and separation performance. This phenomenon could be further confirmed in Fig. S6 (a) and Fig. S9. The sample $NaTaO_3$-E-G2 displayed poorer visible light-harvesting ability than that of sample $NaTaO_3$-E-G2.5 but better visible light induced photocatalytic activity. Therefore, it could be

concluded that among above three factors, the peculiar specific surface played the essential role for high performance of $deNO_x$ ability of the samples. Even so, the much improved visible light ability of samples by C modification was also of great importance; otherwise, the visible light induced photocatalytic performance was impossible due to the wide intrinsic band gap of $NaTaO_3$.

Based on above analysis and discussion, the possible photocatalytic mechanism of C modified $NaTaO_3$ was illustrated in Fig. 11. Under visible light irradiation, the carbonaceous species on the surface of $NaTaO_3$ could be regarded as sensitizer to absorb visible light. In this case, the photogenerated electron enabled to transfer from carbonaceous species to the conduction band (CB) of $NaTaO_3$. Then, the electron in CB would react with O_2 to produce $\cdot O_2^-$. Besides, under the excitation of UV light, in addition to the electron transferred from carbonaceous species, the electron in the valence band (VB) could also be excited to the CB. The photogenerated hole in the VB was able to react with OH^- or absorbed water to produce hydroxyl radicals (·OH). Finally, the above as-produced active radicals $\cdot O_2^-$ and ·OH could be used to reduce or oxidize NO gas to N_2 or NO_3 which could be easily eliminated by water, respectively.[48,49]

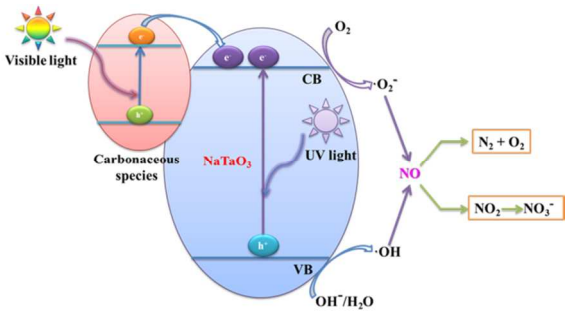

Fig. 11 Possible photocatalytic mechanism of C modified $NaTaO_3$.

Conclusions

Carbon modified $NaTaO_3$ mesocrystal nanoparticles were successfully prepared by a facile solvothermal method by using distilled water/EG as reaction solvent and glucose additive. Due to the co-effect of EG and glucose in the synthesis process of $NaTaO_3$ nanoparticles, the sample presented the large specific surface area and well dispersed mesopores in nanoparticles. The glucose not only played a vital role for controlling the particle size and mesopore volume, but also extremely improved visible light absorption capability. The carbon modified $NaTaO_3$ mesocrystal exhibited outstanding $deNO_x$ performance under the irradiation of UV, short wavelength visible light (>400 nm) and even long wavelength visible light above 510 nm, which was much more effective than those of the sample in the absence of glucose and P25. The prepared $NaTaO_3$ mesocrystal in the present work would probably have a promising application in the areas of environmental cleanup and energy conversion.

Acknowledgements

This research was supported in part by the Management Expenses Grants for National Universities Corporations from the Ministry of Education, Culture, Sports, Science for Technology of Japan (MEXT), the 2014 research Project at the Center for Exploration of New Inorganic Materials (CENIM) in IMRAM Tohoku University, the Grant-in-Aid for Science Research (No. 25289245).

Notes and references

Institute of Multidisciplinary Research for Advanced Materials, Tohoku University, 2-1-1, Katahira, Aoba-ku, Sendai 980-8577, Japan.

* To whom correspondence should be addressed. E-mail: shuyin@tagen.tohoku.ac.jp; Tel: + (00)81-22-217-5599; fax: + (00)81-22-217-5599.

Electronic Supplementary Information (ESI) available: Characterization details about XRD patterns, TEM images, DRS, XPS, FTIR and the corresponding photocatalytic activity of samples. See DOI: 10.1039/b000000x/

1. X. F. Yang, J. L. Qin, Y. Li, R. X. Zhang and H. Tang, *J. Hazard. Mater.* 2013, **261**, 342-350.
2. R. Q. Song and H. Colfen, *Adv. Mater.* 2010, **22**, 1301-1330.
3. H. Colfen and M. Antonietti, *Angew. Chem. Int. Ed.* 2005, **44**, 5576-5591.
4. L. Zhou and P. O'Brien, *Small* 2008, **4**, 1566-1574.
5. L. Zhou and P. O'Brien, *J. Phys. Chem. Lett.* 2012, **3**, 620-628.
6. Z. F. Bian, T. Tachikawa, P. Zhang, M. Fuitsuka and T. Majima, *Nat. Commun.* 2013, doi:10.1038/ncomms4038.
7. S. Kohiki, S. Takada, A. Shimizu, K. Ymada and H. Higashijima, *J. Appl. Phys.* 2000, **87**, 474-478.
8. H. Higashijima, S. Kohiki, S. Takada, A. Shimizu and K. Yamada, *Appl. Phys. Lett.* 1999, **75**, 3189-3191.
9. L. Zhou, D. Smyth-Boyle and P. O'Brien, *J. Am. Chem. Soc.* 2008, **130**, 1309-1320.
10. D. W. Su, S. X. Dou and G. X. Wang, *Nano Res.* 2014, DOI: 10.1007/s12274-014-0440-0.
11. Z. P. Zhang, H. P. Sun, X. Q. Shao, D. F. Li, H. D. Yu and M. Y. Han, *Adv. Mater.* 2005, **17**, 42-47.
12. A. Taden, K. Landfester and M. Antonietti, *Langmuir*, 2004, **20**, 957-961.
13. M. Niederberger and H. CÖlfen, *Phys. Chem. Chem. Phys.* 2006, **8**, 3271-3287.
14. X. Y. Wu, S. Yin, Q. Dong and T. Sato, *Phys. Chem. Chem. Phys.* 2013, **15**, 20633-20640.
15. X. Li and J. L. Zang, *J. Phys. Chem. C* 2009, **113**, 19411-19418.
16. D. R. Liu, Y. S. Jiang and G. M. Gao, *Chemosphere* 2011, **83**, 1546-1552.
17. H. Kato, K. Asakura and A. Kudo, *J. Am. Chem. Soc.* 2003,**125**, 3082-3089.
18. K. Yoshioka, V. Petrykin, M. Kakihana, H. Kato and A. Kudo, *J. Catal.* 2005, **232**, 102-107.
19. Y. G. Su, S. W. Wang, Y. Meng, H. Han and X. J. Wang, *RSC Adv.* 2012, **2**, 12932-12939.

20. J. Y. Shi, G. J. Liu, N. Wang and C. Li, *J. Mater. Chem.* 2012, **22**, 18808-18813.
21. Y. M. Cui, L. Liu, Y. Chen, D. H. Yu, X. F. Zhou, N. P. Xu and W. P. Ding, *Solid State Sci.* 2010, **12**, 232-237.
22. J. X. Sun, G. Chen, J. Pei, R. C. Jin, Q. Wang and X. Y. Guang, *J. Mater. Chem.* 2012, **22**, 5609-5614.
23. S. Yin, M. Komatsu, Q. W. Zhang, F. Saito and T. Sato, *J. Mater. Sci.* 2007, **42**, 2399-2404.
24. S. Liu and J. Yu, *J. Solid. State. Chem.* 2008, **181**, 1048-1055.
25. D. Typke, R. Hegerl and J. Kleinz, *Ultramicroscopy*, 1992, **46**, 157-173.
26. Q. Zhang, S. J. Liu and S. H. Yu, *J. Mater. Chem.* 2009, **19**, 191-207.
27. T. Sugimoto, *Adv. Colloid Interface Sci.* 1987, **28**, 65-108.
28. S. Wohlrab, N. Pinna, M. Antonietti and H. CÖlfen, *Chem. Eur. J.* 2005, **11**, 2903-2913.
29. D. Radziuk, A. Skirtach, G. Sukhorukow, D. Shchukin and H, MÖhwald, *Macromol. Rapid Commun.* 2007, **28**, 848-855.
30. S. Y. Oh, D. I. Yoo, Y. Shin and G. Seo, *Carbohydr. Res.* 2005, **340**, 417-428.
31. D. C. Dragunski and A. Pawlicka, *Mat. Res.* 2001, DOI: 10.1590/S1516-14392001000200006.
32. G. F. Mohamed, M. S. Shaheen, S. K. H. Khalil, A. M. S. Hussein and M. M. Kamil, *Nature and Science* 2011, **9**, 21-31.
33. X. Y. Wu, S. Yin, Q. Dong, C. S. Guo, T. Kimura, J. Matsushita and T. Sato, *J. Phys. Chem. C* 2013, **117**, 8345-8352.
34. Y. Z. Li, D. S. Hwang, N. H. Lee and S. J. Kim, *Chem. Phys. Lett.* 2005, **404**, 25-29.
35. T. Ohno, T. Tsubota, K. Nishijima and Z. Miyamoto, *Chem. Lett.* 2004, **33**, 750-751.
36. B. Neumann, P. Bogdanoff, H. Tributsch, S. Sakthivel and H. Kisch, *J. Phys. Chem. B* 2005, **109**, 16579-16586.
37. X. Y. Wu, S. Yin, Q. Dong, C. S. Guo, H. H. Li, T. Kimura and T. Sato, *Appl. Catal. B: Environ.* 2013, **142-143**, 450-457.
38. Q. Li, J. C. Bian, L. Zhang, R. Q. Zhang, G. Z. Wang and D. H. L. Ng, *ChemPlusChem* 2014, **79**, 454-461.
39. X. M. Sun and Y. D. Li, *Angew. Chem. Int. Ed.* 2004, **43**, 597-601.
40. H. L. Niu, Q. Min, Z. Y. Tao, J. M. Song, C. J. Mao, S. Y. Zhang and Q. W. Chen, *J. Alloys Compd.* 2011, **509**, 744-747.
41. W. Jiang, X. L. Jiao, D. R. Chen, *Int. J. Hydrogen Energy* 2013, **38**, 12739-12746.
42. J. Hussain, K. Palaniradja, N. Algumurthi and R. Manimaran, *J. Eng. Res. Stud.* 2012, **3**, 34-44.
43. D. B. Kittelson, *J. Aerosol Sci.* 1998, **29**, 575-588.
44. A. Fujishima, T. N. Rao and D. A. Tryk, *J Photoch. Photobio C* 2000, **1**, 1-21.
45. R. Quesada-Cabrera, A. Mills and C. O'Rourke, *Appl. Catal. B: Environ.* 2014, **150-151**, 338-344.
46. S. P. Phivilay, A. A. Puretzky, K. Domen and Israel. E. Wachs, *ACS Catal.* 2013, **3**, 2920-2929.
47. B. J. Selby, T. I. Quickenden and C. G. K. Freeman, *Catal.* 2003, **44**, 5-15.
48. C. H. Huang, Y. M. Lin, I. K. Wang and C. M. Lu, *Int. J. Photoenergy*, 2012, **2012**, 1-13.
49. U. Sulaeman, S. Yin and T. Sato, *Appl. Phys. Lett.* 2010, **97**, 103102.

Table of contents entry

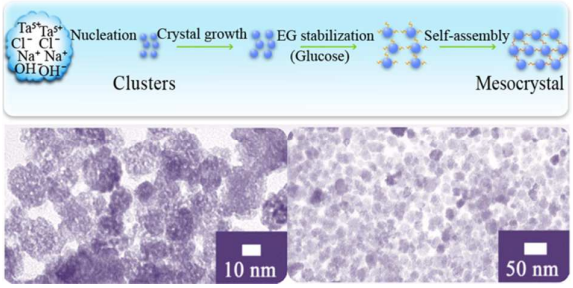

A carbon modified $NaTaO_3$ mesocrystal was successfully prepared by a one-pot solvothermal method, presenting excellent visible light induced deNO_x ability.